Nucleation Simulations Using the Fluid Dynamics Software FLUENT with the Fine Particle Model FPM

Erik Herrmann,*,† Heikki Lihavainen,‡ Antti-Pekka Hyvärinen,‡ Ilona Riipinen,† Martin Wilck,§ Frank Stratmann,|| and Markku Kulmala†

Department of Physical Sciences, University of Helsinki, Finland, Finnish Meteorological Institute, Helsinki, Finland, Particle Dynamics GmbH, Leipzig, Germany, and Leibniz-Institut für Troposphärenforschung, Leipzig, Germany

Received: July 20, 2006; In Final Form: September 7, 2006

This work is an assessment of the capabilities of the FLUENT-FPM software package to simulate actual nucleation experiments. In the first step, we verified the FPM condensation routine with the NEWALC code. Next, homogeneous nucleation of *n*-butanol, *n*-pentanol, and *n*-hexanol in a laminar flow diffusion chamber (LFDC) was simulated and the results were compared to experimental data and an earlier model, which was described by Lihavainen and Viisanen (2001) and will be called femtube2 in the following. Models based on classical nucleation theory typically give too small nucleation rates for alcohol vapors. Also, the FPM underestimates particle production by several orders of magnitude, the factor being a constant for each nucleation isotherm (i.e., at constant nucleation temperature). However, experimental observations beyond exact particle concentrations can be reproduced. We found a behavior similar to the experiment for the dependence of the concentration of nucleated particles *N* on the flow rate. After correcting the FPM nucleation rate by a constant factor, experimentally found vapor depletion effects could be simulated. Comparing the FPM and femtube2, we observed that the FPM systematically predicts lower saturation ratio values. Further investigation of vapor depletion showed significant differences between the FPM and the femtube2 model. Furthermore, FPM simulations confirm the earlier found carrier gas effect (Lihavainen and Viisanen, 2001).

1. Introduction

Ambient aerosols have a significant impact on climate. They serve as a media for atmospheric heterogeneous chemistry and affect the earth radiative balance through light scattering (direct effect) and by acting as condensation nuclei in cloud formation (indirect effect). High aerosol concentrations also decrease the air quality and, thus, affecting human health and visibility. New particle formation in the atmosphere has been observed in various locations and conditions all over the world.[1,2] New particle formation can lead to a significant increase in the number concentration of cloud condensation nuclei[3] therefore affecting the climate. Nucleation, the basic process leading to new particle formation, has been studied theoretically and experimentally for over 100 years. However, it is still poorly understood. Nucleation is still mainly predicted with the classical nucleation theory, which is not able to give quantitatively correct nucleation rates.

Laboratory measurements on nucleation are conducted to understand basic nucleation processes and to develop nucleation theories. However, homogeneous nucleation experiments were shown to yield significantly different results depending on the measuring device used. For example, the nucleation rates of *n*-pentanol and helium measured in a laminar flow diffusion chamber[4] and in a static diffusion chamber[5] can differ by almost 4 orders of magnitude. Another issue in nucleation studies conducted in different measurement devices concerns the carrier gas effect. In diffusion based nucleation devices, the type and the pressure of the carrier gas was observed to have an effect on the nucleation process.[6−8] This is in contradiction to findings observed in pressure dependent nucleation devices.[9−10] It is still an open question whether the carrier gas effect is a real effect or an experimental "feature" of diffusion based nucleation devices.

Given the discrepancy of the results in nucleation measurements, it seems evident that the operational characteristics of different devices should be considered more carefully. One such device is the laminar flow diffusion chamber (LFDC), which utilizes the nonisothermal diffusion in a continuous laminar flow to produce supersaturation of nucleating vapor. An aspect resulting in inaccuracy in all nucleation devices is that nucleation cannot be measured directly; only resulting particle concentrations can be detected after the nucleated particles have grown to detectable sizes. Acquiring quantitative results in the laminar flow diffusion chamber requires the knowledge of the temperature and saturation ratio at the spatial location of the nucleation peak inside the chamber. As these parameters cannot be measured directly, theoretical fluid dynamics models are needed to describe the flow profiles in the chamber. Therefore, the model plays a crucial role in the accuracy of the data analysis.

FLUENT is a flow simulation software whose complex possibilities are available to aerosol modeling through the recently developed fine particle model (FPM). FLUENT−FPM provides full fluid and aerosol dynamics. Because only geometry, materials, and boundary conditions need to be defined, the program is a natural choice to setup an alternative model for error analysis in nucleation measurements. Additionally, FLUENT−FPM is a good candidate to compare different

† University of Helsinki.
‡ Finnish Meteorological Institute.
§ Particle Dynamics GmbH.
|| Leibniz-Institut für Troposphärenforschung.

10.1021/jp064604m CCC: $33.50
Published on Web 10/24/2006

nucleation experiment setups without the need to develop different models. Moreover, such a comparison will be more consistent than a multi-model approach.

The scientific possibilities of the software in the field of particle nucleation have not yet been thoroughly evaluated. As a first step to assess these possibilities, we have simulated a selection of the experiments described in refs 4 and 8. Our objectives are to compare simulated and experimental results where such a comparison is possible. We also re-interpret experimental data with FPM model results and compare the findings to those obtained with the femtube2 model, which is based on classical nucleation theory (as is the FPM). Furthermore, we use FLUENT−FPM to investigate the carrier gas effect.

2. Materials and Methods

2.1. FLUENT. FLUENT (version 6.2.16, Fluent, Inc.) is a commercially available computational fluid dynamics (CFD) software used to calculate the properties of fluid flows. It models flow based on the Euler equations for mass (eq 1) and momentum (eq 2) conservation

$$\frac{\partial \rho}{\partial t} + \nabla\cdot(\rho\vec{v}) = S_{\mathrm{m}} \tag{1}$$

$$\frac{\partial}{\partial t}(\rho\vec{v}) + \nabla\cdot(\rho\vec{v}\vec{v}) = -\nabla p + \nabla\cdot\bar{\tau} + \rho\vec{g} + \vec{F} \tag{2}$$

where S_{m} is a source term, $\bar{\tau}$ is the stress tensor, and $\rho\vec{g}$ and $\vec{F}$ are gravitational and external body force, respectively. As usual, ρ, $\vec{v}$, and p symbolize density, velocity, and pressure, respectively. These two equations are valid for laminar flows. In addition, FLUENT offers various models to include turbulence in the simulations. In this work, however, all considered flows are laminar, and therefore a discussion of these models is not necessary.

FLUENT solves the governing equations using a control-volume-based technique that divides the simulation domain into discrete control volumes, integrates the governing equations on each individual control volume to construct equations for the dependent variables (velocity, pressure, etc.), linearizes the discrete equations, and solves them to obtain updated values of the dependent variables. In our simulations, the software solved the governing equations sequentially (one by one). Because of their nonlinearity, numerous iterations (up to several thousands) of the solution loop are necessary to reach convergence.[11]

2.2. The Fine Particle Model (FPM). FPM (version 1.2.6, Particle Dynamics GmbH & Chimera Technologies) is a particle dynamics model which is added to FLUENT in the form of user-defined functions (UDF). The FPM[12−14] is able to simulate formation, transformation (growth, coagulation), transportation, and deposition of multicomponent particles in gases and liquids. The applicable size range typically stretches from molecule size up to particles in the μm range. Basically, the size is unlimited, but as the FPM simulates the dynamics of a particle population, the FPM criterion has to be met to produce reliable results. It states that a statistically significant number of particles must exist in the simulation domain such that their size distribution can be represented by a continuous function.

The FPM solves the spatial and temporal evolution of a multimodal, multiphase, and multispecies particle size distribution. In FPM 1.2.6, the particle size distribution is represented by a superposition of log-normal size distribution functions (modes). The particle dynamic equations are solved using the moment method in which integral moments of the modes (for example, total number) become additional scalars in FLUENT. Dynamic processes in the current version of the software include coagulation, condensation and evaporation, classical homogeneous nucleation, Brownian and turbulent diffusion, thermophoresis, and gravitational settling. Further processes or different microphysical expressions can be considered by writing user-defined functions for the FPM (FPM-UDF).

The key process in our simulations is homogeneous nucleation. Besides others, the FPM offers a kinetically corrected version of the classical nucleation theory (CNT) formulation by Becker-Döring[15]

$$J_{\mathrm{Becker}} = \frac{(\rho_{\mathrm{g}}\xi_i)^2}{\rho_{\mathrm{i}} w_{\mathrm{i}}}\sqrt{\frac{2\sigma_{\mathrm{i}}}{\pi w_i}}\exp\left(-\frac{\Delta G^*}{k_B T}\right)\cdot\left(\frac{m_p^*}{w_{\mathrm{i}}}\right)^{2/3} \tag{3}$$

where i stands for the nucleating species; the current version of FPM considers only single-component nucleation. The notation in eq 3 is mostly standard; ξ_{i} represents the mass fraction of i in the gas phase, w_{i} is the molecular weight of i, ρ_{g} is the gas density, ρ_{i} is the liquid density of i, and m_p^* is the mass of the critical cluster. There are more recent modifications of the CNT such as the one by Girshick.[16] But since one of our aims in this work is to compare two models, we chose the formulation that is closest to the one used in femtube2.

In our simulations, we expect particle number concentrations of a magnitude where coagulation is negligible. A few test simulations have supported this assumption; thus we neglected coagulation to save computing time. On the other hand, particles are initially very small (ca. 1 nm), which means that particle diffusion and loss to the tube walls have to be taken into account.

2.3. Thermodynamics of *n*-Butanol, *n*-Pentanol, and *n*-Hexanol. Generally speaking, the software considers two different phases: FLUENT, which deals with a mixture of nucleating vapor (*n*-butanol, *n*-pentanol, or *n*-hexanol in our case) and carrier gas (helium or argon), and the FPM, which deals with liquid droplets of nucleated substance. These two species are connected by nucleation, condensation, and evaporation in the FPM. However, they have to be defined separately in FLUENT and the FPM. The definitions for all substances and their properties in this work are taken from the references.[4,8,17,18] Depending on their availability, properties can be defined in different ways for different materials. Mostly, those definitions are polynomials or other explicit expressions. In some cases, we have used built-in FLUENT routines, which require only a few parameters.

As an example, Tables 1 and 2 show the property definitions for *n*-butanol.

3. Simulations

3.1. Condensation. With nucleation as the main simulation interest in this study, it is necessary to test condensation first to evaluate the FPMs accuracy regarding the description of condensational growth processes. To achieve this, a couple of condensation scenarios were calculated with the unary condensation[19] program NEWALC. Generally, the current condensation theory is in good agreement with the experimental findings.[20] NEWALC calculates the growth of particles (in our case *n*-butanol) from a certain initial saturation ratio ($S_{\mathrm{init}} > 1$) until equilibrium conditions ($S = 1$) are reached.

In FLUENT−FPM, one can simulate a similar situation with a simple flow tube. Initial particle size, particle concentration, and saturation ratio are introduced as boundary conditions at the tube inlet. In addition to simply testing condensation, it is possible to simulate effects that would appear in an experimental

TABLE 1: Definition of *n*-Butanol Liquid[a]

molecular mass	$M = 0.074123$
critical temperature	$T_c = 563.05$
critical pressure	$p_c = 44.23 \cdot 10^5$
critical volume	$v_c = 275.0\ \mathrm{cm}^3$
boiling point	$T_b = 390.4$
density	$\rho_{liq} = 990.9563548 - 0.524148\ T - 0.00032\ T^2$
equilibrium vapor pressure	$p_{eq} = \exp(98.494 - 9412.6064\ T^{-1} - 10.54 \ln T)$
surface tension	$\sigma = 4.833 \cdot 10^{-2} - 8.181 \times 10^{-5}\ T$
thermal conductivity	k_{liq}: Sato−Riedel[27]
latent heat	$L = (1.0559 \times 10^6) - 1182.0\ T\ [\mathrm{Jmol}^{-1}]$

[a] All units are SI except where noted.

TABLE 2: Definition of *n*-Butanol Vapor[a]

density	ρ_{vap}: ideal gas
molar mass	$M = 0.074123$
specific heat	$c_p = 44.0619 + 5.6393T - 0.003025T^2 + (6.3206 \times 10^{-7})T^3$
thermal cond.	$k_{vap} = (-7.772 \times 10^{-3}) + (3.564 \times 10^{-5})T + (1.206 \times 10^{-7})T^2 - (4.992 \times 10^{-11})T^3$
viscosity	$\eta_{vap} = (-1.843 \times 10^8) + (2.867 \times 10^6) - 104.8$
diffusion coeff.	$D = 1.48313 \times 10^{-9} T^{1.75}/P_{tot}$, where P_{tot} is in bars

[a] Diffusion coefficient is valid for a mixture of helium and *n*-butanol vapor. All units SI, except were noted.

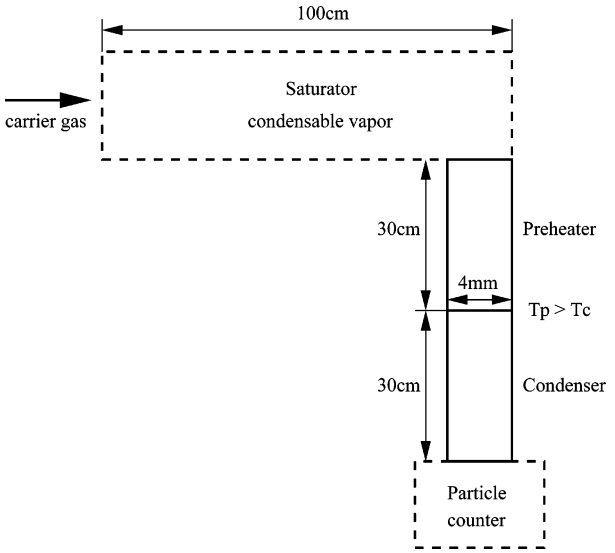

Figure 1. Schematic figure of the experimental setup.

setup. For example, the vapor depletion to the walls (by defining additional wall boundary conditions) will result theoretically in a smaller, final particle size than predicted by NEWALC. Furthermore, we are able to consider particle losses by diffusion to the walls, by coagulation, or by sedimentation. Generally, we expect good FLUENT−FPM results for condensation simulations because the moment method (as used by the FPM) is most accurate for condensation processes.

3.2. Nucleation. *3.2.1. A Nucleation Experiment.* The central part of this work is the simulation of a nucleation experiment. The experimental work underlying our simulations has been described in ref 8. Figure 1 shows the experimental setup schematically. First, an inert carrier gas is saturated in a saturator (length ca. 1 m) with the nucleating vapor, then the mixture enters the preheater ($T_{preheater} > T_{saturator}$), and finally it enters the condenser ($T_{condenser} < T_{saturator}$). The preheater and the condenser are each ca. 30 cm long with an inner diameter of 4 mm. The preheater and the condenser are thermally insulated from each other to ensure a stepwise temperature drop at the wall of the junction. Because equilibrium vapor pressure is an exponential function of temperature, and for the investigated species, heat transfer is faster than mass transfer of the nucleating vapor, supersaturation is achieved in the condenser with the saturation ratio maximum on the centerline of the condenser tube. Saturation ratio S is mainly controlled by the temperature of the saturator, and nucleation temperature is controlled by the temperatures of the preheater and the condenser. For large enough values of S, homogeneous nucleation occurs inside the condenser tube (i.e., liquid drops form from vapor). Nucleated particles are counted after the condenser where they have typically grown to diameters of a few mm.

3.2.2. Realization in FLUENT−FPM. Even though the experimental setup is rather simple, it needs to be further simplified for a simulation in FLUENT. The main motivation is the necessity to minimize the computing time without losing accuracy where it is really needed (i.e., in the volume around the nucleation maximum), which in most of our simulations is a few centimeters into the condenser.

The FLUENT simulation (Figure 2) considers only the preheater and the condenser. The properties (temperature, mass flow rate, and mass fractions) of the saturated mixture of carrier gas and vapor coming from the saturator are introduced as a boundary condition at the tube inflow. Also, the simulated preheater is only 10 cm long; tests have shown that flow, temperature, and saturation ratio profiles are completely developed in a few centimeters after the preheater inlet. Furthermore, the simulated condenser is longer than 30 cm. This is a precaution to keep simulation boundary effects at the tube outflow from influencing the 30 cm length of the true experimental condenser. The walls of the preheater and the condenser are set to the same temperature as in the actual experiment. To account for vapor losses to the walls, the mass fraction of the nucleating vapor at all of the walls is set to match a saturation ratio of 1 at wall temperature. Altogether, the simulation volume consists of ca. 200 000 cells. These cells are particularly small at the beginning (ca. 5 cm) of the condenser because test simulations have shown that the exact determination of the nucleation maximum value and location is sensitive to grid coarseness.

4. Results and Discussion

4.1. Simulation Data. FLUENT−FPM delivers data sets of flow velocity, saturation ratio, and particle concentration (among others) for the whole simulation domain. However, the maximum experimental nucleation rate J_{exp}^{max} is normally used as the resulting nucleation rate from flow chamber experiments, and thus it is the logical choice for comparison of our simulations and earlier theoretical results. The use eq 4 to obtain J_{exp}^{max}

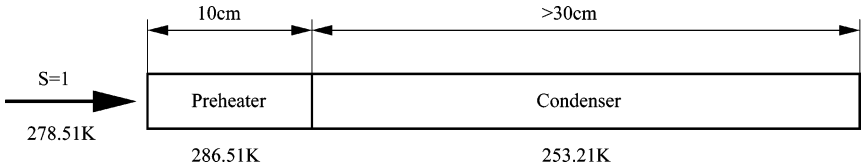

Figure 2. Schematic figure of the simulation setup. The temperature values (K) are examples taken from actual simulations to illustrate typical temperature values and relations in different parts of the setup. Note that the condenser is longer than in real life to suppress boundary effects in the simulation at the tube outflow. The actual vertical orientation of the experimental setup as shown in Figure 1 is simulated by defining the direction of gravitation accordingly.

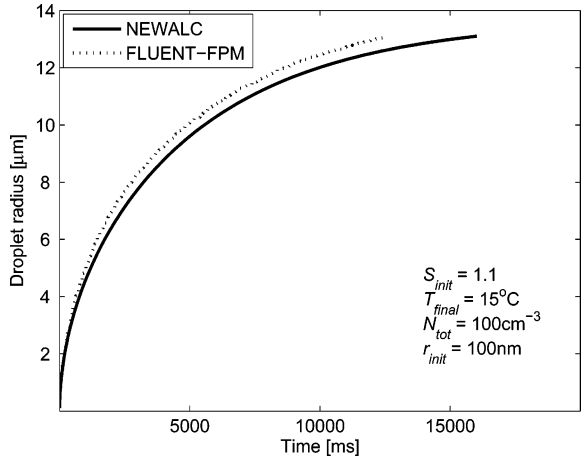

Figure 3. Condensation of butanol to butanol particles under the specified conditions in FLUENT−FPM and in the unary condensation model NEWALC. Note that T_{final} is 15 °C only for NEWALC; in FLUENT, this is the initial temperature.

from a LFDC has been proposed.[21]

$$\frac{J_{exp}^{max}}{\int J_{exp} dV} = \frac{J_{theo}^{max}}{\int J_{theo} dV} \tag{4}$$

For our purposes this becomes

$$J_{exp}^{max} = J_{theo}^{max} \frac{N_{exp}}{N_{theo}} \tag{5}$$

where J_{theo}^{max} is the maximum theoretical nucleation rate on the central axis of the simulation tube. FPM gives the nucleation rate for each cell. Alternatively, J_{theo}^{max} can be calculated from the flow velocity (in direction of the tube axis) and particle concentration N. Both approaches yield identical results. N_{exp} is the particle concentration number measured in the actual experiment, whereas N_{theo} is the particle concentration number an instrument would count downstream of the simulated condenser. N_{theo} is the average of particle concentrations (weighed with the flow velocity in each respective cross-section cell) over the condenser cross-section at 30 cm from the beginning of the condenser.

4.2. Simulation Results. *4.2.1. Condensation.* Figure 3 shows the growth of *n*-butanol particles caused exclusively by condensation for simulations with FLUENT−FPM and the unary condensation model NEWALC over a time span of 12 s. The carrier gas is air. We find good agreement between the two models with final radii (at 12 s) of ca. 12.5 and 13 μm for NEWALC and FLUENT-FPM, respectively.

The remaining difference is partly caused by the different modeling approaches; a time-dependent zero dimensional (0D) model like NEWALC is compared to a time-independent two dimensional (2D) simulation. More important still is a fundamental difference in the setup. In NEWALC, the final temperature is 288K. For lack of better data, that number was used as the initial temperature in FLUENT. The difference is small (about 0.3 K), but at the same saturation ratio the FLUENT calculation contains more vapor, and thus leading to bigger particles.

4.2.2. FPM Verification. Before attempting to evaluate experimental data, it is necessary to verify that the FPM produces reasonable results. To achieve this, we have simulated two sets of experiments that were initially carried out to test LFDC operation.[4] These experiments studied the dependence of measured particle concentration, N, on saturator temperature and flow rate. They are suitable for a comparison of simulation and experiment as all quantities in the experiment can be measured directly.

With growing temperature gradient between the saturator and the condenser, experimentally observed particle concentrations will initially grow according to the theoretically possible saturation ratio of the setup and the resulting nucleation rates. There is, however, a point after which the measured particle concentration and, thus, the nucleation rate will no longer grow. Based only on the temperature difference and the expected saturation ratio, higher nucleation rates would be expected. In the experiment, however, only a limited amount of vapor is available to form new particles, and this limits particle production possibilities.

When simulating alcohols, classical nucleation theory typically underestimates nucleation rates significantly.[22−23] As the FPM in the form used here utilizes a CNT nucleation rate expression, nucleation rates calculated by the FPM are no exception. This means that it will not be possible to reproduce the vapor depletion effect without correcting the nucleation rate in such a way that N_{theo} matches the experimental values. N_{exp}/N_{theo} is approximately constant for constant T_{nuc}. This means we can determine N_{exp}/N_{theo} for small N_{exp} when vapor depletion is negligible, that is, when N_{exp} grows exponentially. The resulting coefficient then can be used as a nucleation correction factor in the FPM to examine vapor depletion for large N_{exp} on the same nucleation isotherm.

Figure 4 displays a series of calculations of N_{theo} with a steadily rising $T_{saturator}$ and compares FPM calculation results directly to experimental data. The nucleating vapor is *n*-pentanol and the carrier gas is helium. In all of these simulations, the nucleation correction factor described above has been applied to the nucleation rate used. For these calculations, only the $T_{saturator}$ and the respective *n*-pentanol vapor mass fraction were altered. All other parameters and boundary conditions were fixed and T_{nuc} was approximately constant (270 K). The nucleation correction factor is 100 000. We see that the roughly exponential relation between N_{theo} and $T_{saturator}$ ends at around $T_{S1} = 296$ K. The curve becomes more flat because of vapor depletion, showing a behavior similar to the experiment. For very large N_{exp}, we see that the FPM somewhat overestimates particle production in comparison to the experiment. This difference probably is caused by limitations of the experimental system,

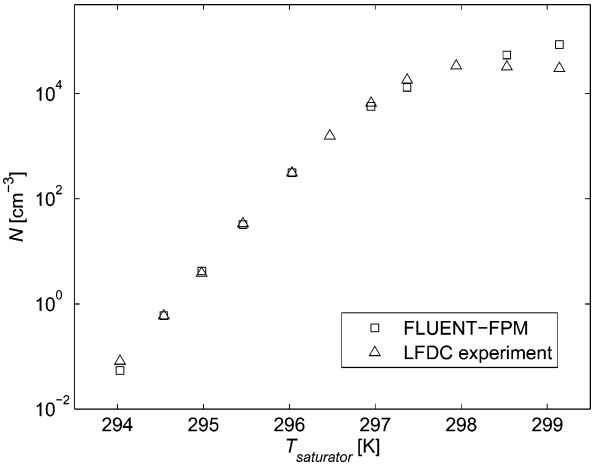

Figure 4. Dependence of particle concentration N_{theo} at the tube outlet on $T_{\text{saturator}}$. While vapor depletion is negligible and all other parameters are constant, $T_{\text{saturator}}$ alone determines S.

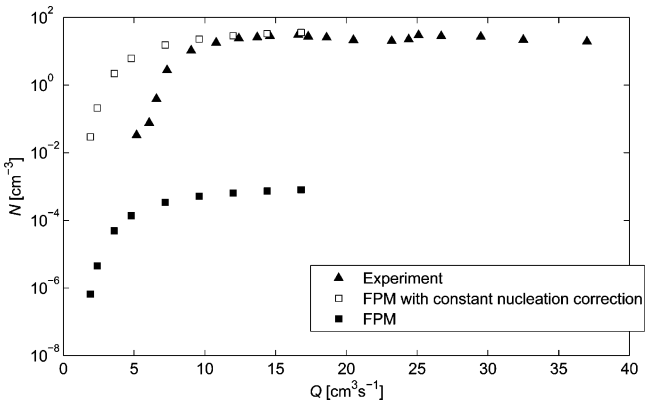

Figure 5. Dependence of particle concentration N on flow rate Q for *n*-pentanol. Simulation results recalculated with a constant nucleation correction factor of 45 000 to match the order of magnitude of theoretical and experimental results and thus illustrate the offset for small particles more clearly.

and its counting efficiency is decreased significantly when particle concentration is higher than 10^4cm^{-3}. We also have neglected the liquid film on the condenser wall in all our simulations. With so much vapor available, this film could have a certain effect. A more detailed analysis of the implications of a liquid film in a completely different simulation setup would be necessary to evaluate this.

The flow rate affects the temperature and saturation ratio profiles in the LFDC and thus influences nucleation rates and particles concentration N. Figure 5 shows the effect in the experimental situation and our simulation results. The example depicts the dependence of N on flow rate Q for the nucleation of *n*-pentanol in helium. Of course, both curves do not coincide, simply because the FPM systematically underestimates nucleation rates as was already mentioned above and will be discussed in detail later on. However, we are able to reproduce the basic shape of the experimental curve, although it is shifted down by some orders of magnitude. Through the use of the same nucleation correction method as above, it becomes clear that the theoretical nucleation appears to start at lower flow rates. The constant nucleation correction factor for these additional calculations was taken from the data for Figure 6, at a nucleation temperature of roughly 260K it is 45 000. Femtube2 has produced a similar shift effect for *n*-pentanol[17] and *n*-hexanol.[8]

4.2.3. Evaluation of Experimental Data. Nucleation was simulated for *n*-butanol, *n*-pentanol and *n*-hexanol. For each

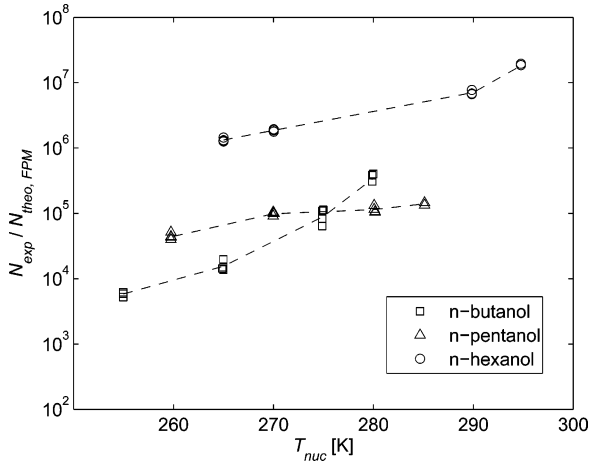

Figure 6. The ratio $N_{\text{exp}}/N_{\text{theo}}$ in relation to nucleation temperature T_{nuc}. Dashed lines serve to guide the eye.

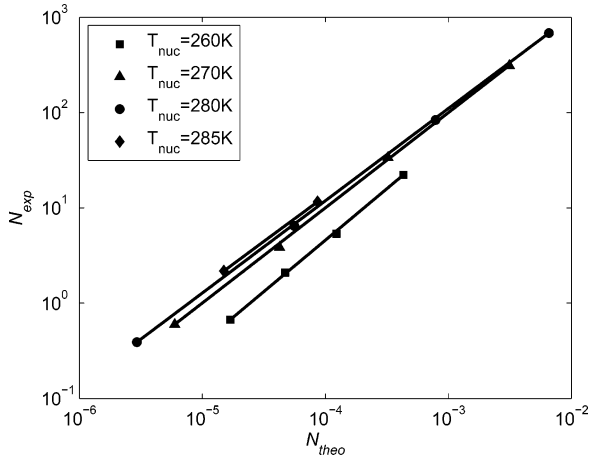

Figure 7. Experimental particle concentration N_{exp} as a function of theoretical values N_{theo} for *n*-pentanol at various nucleation temperatures. Straight lines of the form $\log(N_{\text{exp}}) = A + B \log(N_{\text{theo}})$ have been fitted to the data.

vapor, three isotherms[4,8] were chosen for FPM runs to cover the full range of nucleation temperatures in the experiments. Figure 6 shows the $N_{\text{exp}}/N_{\text{theo}}$ ratio depending on saturator temperature for all simulated isotherms.

The FPM systematically underestimates particle production as Figure 6 illustrates. This is typical if the CNT expressions are used to determine the nucleation rates for alcohols, and this also has been found in the case of femtube2. For *n*-pentanol, we observe $N_{\text{exp}}/N_{\text{theo}}$ to be almost constant over the available range of nucleation temperatures T_{nuc}. The *n*-hexanol shows a slight growth of $N_{\text{exp}}/N_{\text{theo}}$ with rising T_{nuc}. The ratio for *n*-butanol depends very strongly on T_{nuc}. Figure 6 also shows that $N_{\text{exp}}/N_{\text{theo}}$ is almost constant for constant T_{nuc}; all ratios for a certain nucleation temperature (i.e., belonging to one isotherm) are "clustered" very close to one another. This has been used, for example, in the determination of the nucleation correction factor needed for the vapor depletion simulations described above.

Of the vapors used, *n*-pentanol is the only one to exhibit an almost constant $N_{\text{exp}}/N_{\text{theo}}$ ratio (i.e., the only one to be described reasonably well by CNT). Therefore, we will have a closer look at the pentanol simulations and experiments. Figure 7 shows a direct comparison of N_{exp} and N_{theo}. A straight line of the form

$$\log_{10}(N_{\text{exp}}) = A + B \log_{10}(N_{\text{theo}}) \tag{6}$$

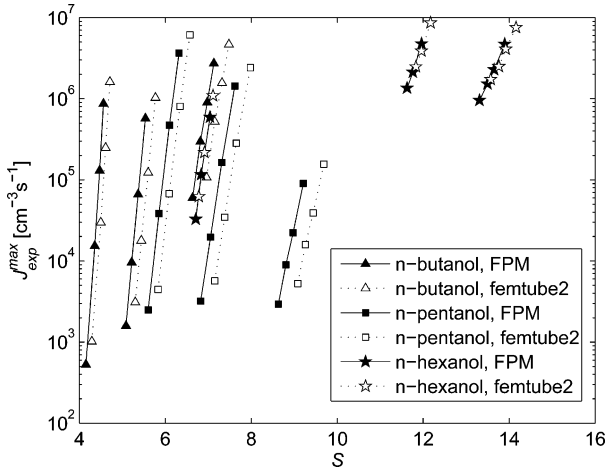

Figure 8. Three nucleation isotherms for *n*-butanol, *n*-pentanol, and *n*-hexanol for both FPM and femtube2.

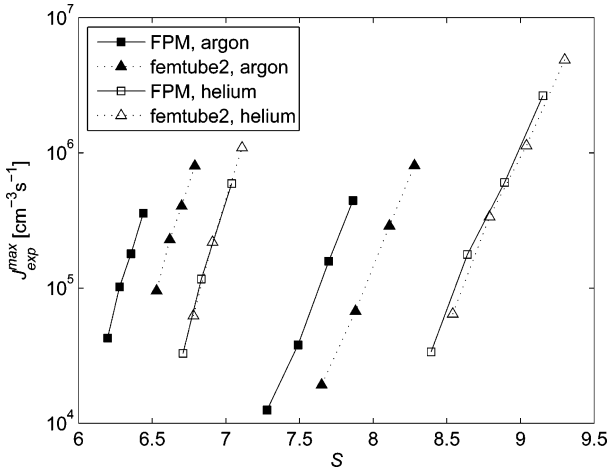

Figure 9. Nucleation of *n*-hexanol with helium and argon as carrier gases. Nucleation temperature for the four isotherms: on the left, $T_{nuc} = 290$ K, and on the right, $T_{nuc} = 280$ K.

was fitted to the data points from each isotherm. If experimental results match the used theory, the slopes of these lines should be one, and the intercepts should be zero. For the slopes of the four lines in Figure 7, we found an average value of 1.00 with a standard deviation of 0.03. This means that the theory captures the experimental saturation ratio dependence. For the intercepts, we found an average value of 4.96 with a standard deviation of 0.02. This means that the theory and the experiment disagree by about 5 orders of magnitude on the absolute number of particles. This is even larger than the difference found with femtube2, which was about 3.2. However, the femtube2 result also shows that large differences between experiment and theory are typically found.

For hexanol and butanol, one finds similar pictures with straight lines for each isotherm. Also, the slopes are around one ($1.03 \pm 0.02$for butanol and 0.98 ± 0.02 for hexanol). However, intercepts vary greatly (2.69 ± 0.84 for butanol and 4.58 ± 0.91 for hexanol), growing as a function of T_{nuc} as Figure 6 would suggest.

As mentioned above, J_{theo}^{max} is the typical quantity to evaluate experimental results. Figure 8 shows three isotherms for each of the three vapors, and helium is the carrier gas in all cases. Figure 8 also includes femtube2 results. The comparison between J_{exp}^{max} (femtube2) and J_{exp}^{max} (FPM) shows that the results are rather similar. Figure 8 shows that the FPM systematically predicts smaller saturation ratios than femtube2. This can be caused by a number of reasons. Those reasons will be addressed in the following comparison of the models. To explain the different magnitudes of deviation of saturation ratios *S* for different materials (*n*-butanol 2−5%, *n*-pentanol 3−5%, *n*-hexanol 1−2%), one also has to consider the different implementations of physical properties for different materials that depend on the mathematical form in which those properties are available.

A carrier gas effect for LFDC experiments of hexanol nucleation was reported[8]: analysis of experimental data with femtube2 resulted in different isotherm locations at the same nucleation temperature depending on the used carrier gas. However, it is unclear whether this is a real effect or a product of the model used for analysis. Figure 9 shows that FLUENT−FPM reproduces this effect. As shown above, the FPM curves are shifted toward smaller values of *S*, but our simulations essentially confirm the earlier findings. In these simulations, we had to use a different grid, because the nucleation maximum is located relatively far from the beginning of the condenser. Also the *S* profile is very wide, which leads to a longer "volume of interest", and thus the need to choose a coarser grid. This, at least partly, accounts for the larger differences in *S*. Additionally, the way toward the nucleation maximum is now longer, and the flow velocity is lower. This means more time for the processes that we suspect cause the differences that will be discussed in the following.

4.2.4. Differences Between FPM and Femtube2. As seen above, FPM and femtube2 produce quite similar results and show the same behavior in many setups. However, Figure 8 also depicts that the FPM systematically predicts smaller values for the saturation ratio S_{max} at nucleation rate maximum. The difference appears to be growing with *S*. For this, three possible reasons have been identified. First of all, there is the issue of grid resolution. All values that FLUENT delivers are averages over a certain volume, and not values at one exact location. Considering how narrow the *S* profile is in space, this will cause a somewhat smaller *S* value than the one exactly at the tube center. Second, femtube2 assumes a laminar (parabolic) and constant velocity profile at all times with flow only in the direction of the tube central axis. However, the flow velocity is not constant throughout the tube. The mass flow is constant, and because of the cooling of the gas, the flow velocity decreases. This change is approximately proportional to the temperature decrease, as it should be according to the ideal gas law. The above analysis of the relationship of particle number concentration *N* and flow rate *Q* has shown that *S* is lower for smaller flow rates. Thus, the decrease in flow rate can partly explain the *S* differences between the FPM and femtube2. However, this effect is rather small.

A more significant effect that causes the *S* shift between femtube2 and the FPM is the different way both models handle vapor depletion to nucleated particles. The FPM includes vapor depletion at every step of the way, whereas femtube2 does not consider it at all. The effect is noticeable for moderate values of *S*, but it becomes significant at very high saturation ratios. Figure 10 contains the same set of data as Figure 4, only this time analyzed from a J_{exp}^{max} point of view. While femtube2 sees a continued rise of *S* while J_{exp}^{max} stagnates, the FPM shows an upper limit for both. Moreover, the FPM result fits classical nucleation theory predictions as the data points remain on a (roughly) straight line. Figure 8 illustrates how the FPM interprets nucleation in the LFDC: instead of calculating nucleation rates as function of temperature and saturation profiles based on heat and vapor mass transfer only,

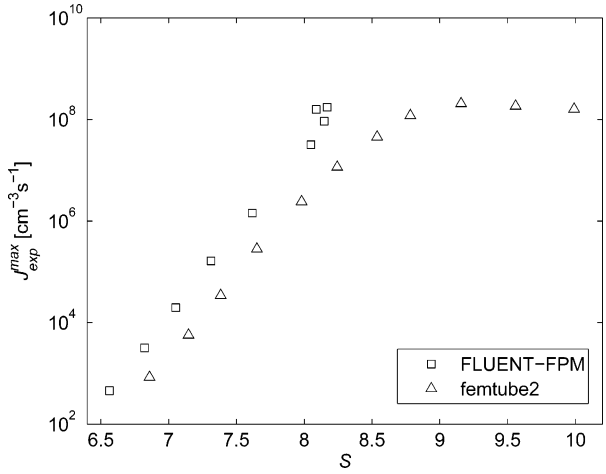

Figure 10. Vapor depletion. J_{exp}^{max} comparison of FLUENT-FPM and femtube2.

(i.e., neglecting the vapor depletion to the particles) the FPM accounts for this feedback of particle dynamics on the heat and mass transfer. In other words, the temperature and saturation profiles and, consequently, the nucleation rates are determined, accounting for the reduction of vapor due to the condensational sink introduced by the particles. At moderate S values, the effect of vapor depletion to the particles is small (ΔS around 0.1). For extreme temperature gradients between the preheater and the condenser, however, the effect on the saturation ratio profile becomes important. Vapor is consumed by particle formation and growth before the theoretically possible (i.e., without depletion) maximum values of S can be reached. With the same logic, the FPM also predicts the nucleation rate maximum to be located closer to the beginning of the condenser (ca. 2.3 cm for the highest simulated values of $T_{saturator}$) than according to femtube2 in which the location of the nucleation maximum is nearly constant (ca. 3.3 cm into the condenser).

Figure 8 also shows that values for J_{exp}^{max} are lower when the FPM delivers the theoretical data. Ideally, J_{exp}^{max} should be independent of the used model. However, with S being lower, we cannot expect to reproduce the same J_{exp}^{max}. With T_{nuc} being roughly the same in both models, J_{exp}^{max} for FPM and femtube2 should nevertheless be located on the same isotherm if both models work similarly. Because FLUENT−FPM also considers particle losses to the walls, this affects N_{theo} and thus J_{exp}^{max}. Freshly nucleated particles are likely to be removed efficiently because of their very small diameter. To estimate the order of magnitude of these losses, we performed a couple of simple simulations with particles of uniform size in a tube of 4 mm diameter. The flow rate was the same as in the actual nucleation simulations. Of 1 nm particles, over 30 were lost after travelling only 1 cm. For 10 nm particles, the loss rate was 2.5%. Additionally, a closer inspection of simulation results in both models shows slightly differing J profiles that will add to the difference in the J_{theo}^{max}/N_{theo} ratio and move FPM and femtube2 results to their own respective isotherms.

5. Conclusions

In this work, we have used the FLUENT−FPM software to simulate LFDC experiments on the nucleation of *n*-butanol, *n*-pentanol, and *n*-hexanol in helium. Additionally, the nucleation of *n*-hexanol in argon was investigated. The simulation mesh geometry was chosen to be as fine as possible in the volume around the nucleation maximum while also considering computational limitations. The properties of the working materials (vapors, carrier gases) and the formulation of nucleation were defined to match earlier calculations with femtube2 as closely as possible. The results were analyzed in three steps. First, we compared them directly to experimental data. This offered a possibility to verify the simulation setup in FLUENT−FM. The main focus, however, was on the reevaluation of the data analysis that previously had been carried out with femtube2. To do this, we simulated selected nucleation isotherms to cover a wide range of nucleation temperatures. Also the carrier gas effect was examined. Finally, based on the results from the previous steps, the two different simulation approaches were compared.

Experimental tests on the dependency of particle concentration on the flow rate and the saturator temperature offered an opportunity to compare simulation and experiment directly. The simulated dependence of particle concentration N on flow rate Q is very close to experimental findings. Again, absolute numbers do not match, but the general behavior is rather similar. Closer inspection shows that simulated nucleation starts at somewhat lower flow rates than in the experiment. However, this is likely to be caused by experimental limitations that detect the very large particles at low Q. Deposition of those particles before they can be counted after the condenser is not yet part of either of the two models. The second direct comparison was performed on the basis of vapor depletion experiments. After scaling the FPM nucleation rate to match N_{theo} and N_{exp} under normal conditions, simulations that were closely reproduced measured number concentrations for very high saturator temperature (i.e., high potential saturation ratios).

Similar to femtube2, the FPM systematically underestimates particle production by several orders of magnitude as it utilizes a CNT nucleation rate expression. For the nucleation of *n*-pentanol in helium, the ratio of N_{exp} and N_{theo} is almost constant over the simulated range of nucleating temperatures. For *n*-butanol and *n*-hexanol, we found a noticeable depence on T_{nuc}, which was most pronounced in the *n*-butanol case. However, for all nucleating vapors, we found that the theory captures the experimental saturation ratio dependence quite well.

FLUENT−FPM also reproduced the nucleation isotherms of the original analysis quite well. Generally, the FPM predicts a lower S_{nuc} than femtube2. The differences vary between the substances; however, they never exceed 5%. Reasons for this are vapor depletion to particles, minor differences in the material definitions, a limited grid resolution, and the fact that femtube2 assumes the velocity profile to be constant while there is a significant change in flow velocity at the beginning of the condenser. The FPM also places J_{exp}^{max} on another isotherm. Reasons for this are differences in the J profiles and the inclusion of particle loss processes in the FPM calculations.

Generally, the FPM shows good agreement with experimental data. It confirms certain findings of femtube2 while modifying others by considering additional processes. Our results imply that simplifications usually made in models describing LFDC are not always valid and might cause significant differences in both saturation ratios and nucleation rates calculated from experimental results.

However, the additional processes accounted for in the FLUENT−FPM simulations cannot explain the carrier gas effect. We see that J is higher in the argon case when the nucleation of *n*-hexanol in helium and in argon are compared.[8] Recently, a carrier gas pressure effect also has been demonstrated for the laminar flow diffusion chamber.[24] The effect of the carrier gas and its pressure on nucleation rates is not fully understood, which makes it a suitable subject for closer

investigation using the FLUENT−FPM tool. As similar effects have been observed in a thermal diffusion cloud chamber (TDCC),[5,25−26] this other diffusion-based nucleation device is a good candidate for further investigations, because it was reported that the TDCC gave nucleation rates that were 4 orders of magnitude smaller than in the LFDC.[5] These differences have not been thoroughly investigated as was pointed out earlier.

References and Notes

(1) Kulmala, M. How particles nucleate and grow. *Science* **2003**, *302*, 1000−1001.

(2) Kulmala, M.; Vehkamäki, H.; Petäjä, T.; Dal Maso, M.; Lauri, A.; Kerminen, V.-M.; Birmili, W.; McMurry, P. H. Formation and growth rates of ultrafine atmospheric particles: a review of observations. *J. Aerosol Sci*. **2004**, *35*, 143−176.

(3) Lihavainen, H.; Kerminen, V.-M.; Komppula, M.; Hatakka, J.; Aaltonen, V.; Kulmala, M.; Viisanen, Y. Production of potential cloud condensation nuclei associated with atmospheric new-particle formation in northern Finland. *J. Geophys. Res.* **2003**, *108*, 4782.

(4) Lihavainen, H.; Viisanen, Y.; Kulmala, M. Homogeneous nucleation of *n*-pentanol in a laminar flow diffusion chamber. *J. Chem. Phys*. **2001**, *114*, 10031−10038.

(5) Rudek, M. M.; Katz, J. L.; Vidensky, I. V.; Zdimal, V.; Smolik, J. Homogeneous nucleation rates of *n*-pentanol measured in an upward thermal diffusion cloud chamber. *J. Chem. Phys*. **1999**, *111*, 3623−3629.

(6) Vohra, V.; Heist, R. H. The flow diffusion chamber: A quantitative tool for nucleation research. *J. Chem. Phys.* **1996**, *104*, 382−395.

(7) Hämeri, K.; Kulmala, M. Homogeneous nucleation in a laminar flow diffusion chamber: The effect of temperature and carrier gas on dibutyl phthalate vapor nucleation rate at high supersaturations. *J. Chem. Phys*. **1996**, *105*(17), 7696−7704.

(8) Lihavainen, H.; Viisanen,Y. A laminar flow diffusion chamber for homogeneous nucleation studies. *J. Phys. Chem. B* **2001**, *105*, 11619−11629.

(9) Viisanen, Y. Strey, R.; Reiss, H. Homogeneous nucleation rates for water. *J. Chem. Phys*. **1993**, *99*, 4680−4692.

(10) Grassmann, A.; Peters, F. Homogeneous nucleation rates of *n*-propanol in nitrogen measured in a piston-expansion tube. *J. Chem. Phys.* **2002**, *116*, 7617−7620.

(11) *FLUENT*. *Fluent 6.0 User's Guide*, Fluent Inc.: Lebanon, NH, 2001.

(12) Wilck, M.; Stratmann, F.; Whitby, E. R. *Particle Dynamics. Fine Particle Model* (*FPM 1.2.6*) *Users Guide*, Particle Dynamics GmbH: Leipzig, Germany, 2005.

(13) Wilck, M. *Modal Modelling of Multicomponent Aerosols*; Verlag für Wissenschaft und Forschung: Berlin, Germany, 1999.

(14) Wilck, M.; Stratmann, F.; Whitby, E. R. In *A Fine Particle Model for FLUENT: Description and Application*; Wang, C.-S., Ed.; Sixth International Aerosol Conference, 2002 IAC: Chinese Association for Aerosol Research in Taiwan, 2002.

(15) Courtney, W. G. Remarks on homogeneous nucleation. *J. Chem. Phys.* **1961**, 35, 2249.

(16) Girshick, S. L.; Chiu,C.-P. Kinetic nucleation theory: A new expression for the rate of homogeneous nucleation from an ideal supersaturated vapor. *J. Chem. Phys.* **1990**, *93*, 1273−1277.

(17) Lihavainen, H. A. Laminar Flow Diffusion Chamber for Homogeneous Nucleation Studies. Ph.D. Thesis, University of Helsinki, Helsinki, Finland, 2000.

(18) Yaws, C. L. *Chemical Properties Handbook*; McGraw-Hill: New York, 1999.

(19) Kulmala, M.; Vesala, T. Condensation in the continuum regime. *J. Aerosol Sci*. **1991**, *22*, 337−346.

(20) Vesala, T. Kulmala, M.; Rudolf, R.; Vrtala, A.; Wagner, P. E. Models for condensational growth and evaporation of binary aerosol particles. *J. Aerosol Sci*. **1997**, *28*, 565−598.

(21) Wagner, P. E.; Anisimov, M. P. Evaluation of nucleation rates from gas flow diffusion chamber experiments. *J. Aerosol Sci*. **1993**, *24*, S103−S104.

(22) Gharibeh, M. Kim, Y.; Dieregsweiler, U.; Wyslouzil, B. E.; Ghosh, D.; Strey, R. Homogeneous nucleation of *n*-propanol, *n*-butanol, and *n*-pentanol in a supersonic nozzle. *J. Chem. Phys*. **2005**, *122*, 45121−45129.

(23) Hyvärinen, A.-P.; Lihavainen, H.; Viisanen, Y.; Kulmala, M. Homogeneous nucleation rates of *n*-alcohols in a laminar flow diffusion chamber. *J. Chem. Phys*. **2004**, *120*, 11621−11633.

(24) Hyvärinen, A.-P.; Brus, D.; Zdimal, V.; Smolik, J.; Kulmala, M.; Viisanen, Y.; Lihavainen, H. The carrier gas pressure effect in a laminar flow diffusion chamber, homogeneous nucleation of *n*-butanol in helium. *J. Chem. Phys*. **2006**, *124*, 43041−430411.

(25) Zdimal, V.; Smolik, J. Homogeneous nucleation rate measurements in 1-pentanol vapor with helium as a buffer gas. *Atmos. Res.* **1998**, *46*, 391−400.

(26) Brus, D.; Zdimal, V.; Stratmann, F. Homogeneous nucleation rate measurements of 1-propanol in helium: The effect of carrier gas pressure. *J. Chem. Phys*. **2006**, *124*, 43061−430614.

(27) Reid, R. C.; Prausnitz, J. M.; Poling, P. E. *The Properties of Gases and Liquids*; McGraw-Hill: New York, 1987.